Korean J. Chem. Eng., 39(10), 2875-2882 (2022)
DOI: 10.1007/s11814-022-1183-3

pISSN: 0256-1115
eISSN: 1975-7220

Prediction of defluidization behavior using particle apparent viscosity

Zhuoqing An*,,***,†, Haoran Wang****, and Yanling Zhang*****

*Key Laboratory of Integrated Exploitation of Bayan Obo Multi-Metal Resources,
Inner Mongolia University of Science and Technology, Baotou 014010, China
**Collaborative Innovation Center of Integrated Exploitation of Bayan Obo Multi-Metal Resources,
Inner Mongolia University of Science and Technology, Baotou 014010, China
***School of Materials and Metallurgy, Inner Mongolia University of Science and Technology, Baotou 014010, China
****Department of Quantum Science and Energy Engineering, Graduate School of Engineering,
Tohoku University, Sendai 9808579, Japan
*****State Key Laboratory of Advanced Metallurgy, University of Science and Technology Beijing, Beijing 100083, China
(*Received 28 February 2022 • Revised 29 April 2022 • Accepted 18 May 2022*)

Abstract−The commercial utilization of fluidized beds is usually limited by particle agglomeration and subsequent defluidization. In this paper, a new mathematical model based on force balance is proposed to predict the defluidization behavior of particles in fluidized beds. In this model, the cohesive forces between particles are characterized using particle apparent viscosity and the separating force is mainly determined by the drag force. When the cohesion force was equal to the separating force at different fluidization condition, the minimum fluidization velocity and defluidization temperature were obtained by the model. Further, the fluidization behavior of copper particles including the minimum fluidization velocity and the temperature under which defluidization occurred was examined in a laboratory's fluidized bed reactor. Compared with the experimental data, the results predicted by the model represent good agreement.

Keywords: Apparent Viscosity, Force Balance, Prediction Model, Defluidization Temperature, Minimum Fluidization Velocity

INTRODUCTION

Fluidized beds are ideally suited to treating finely sized materials because they offer good solid mixing, higher heat transfer, and large contact surface area [1,2]. However, widespread use of fluidized beds is limited by solid flow phenomena such as particle agglomeration and subsequent defluidization [3,4]. The large bonding forces between newly formed metal phases cause the particles to pack together under high temperature, further leading to serious sticking of particles, and defluidization [5,6].

Numerous previous studies [7-9] have studied the factors affecting defluidization, which include temperature, gas composition, material species, fluidizing velocity, and particle shape and size. While the particle agglomeration mechanism is still unclear, several models have been proposed to describe the defluidization behavior of particles. Lin et al. [10] used force balance and mass balance combined with regression analysis to establish an agglomeration model to predict defluidization time. Valverde et al. [11] developed a model to predict agglomerate size based on the balance between inter-particle adhesive force and the local shear force acting on the particle in the surface of the agglomerate. Seville [12] and Knight [13] successfully predicted the relationship between the temperature and gas velocity required to inhibit defluidization as a function of the activation energy for surface diffusion. These models only consider the surface/volume diffusion or chemical reaction and melting of the bed material and ignore the motion of actual particles. However, the mixed particles did not have enough contact time to form a sintered neck in a fluidized bed, so the adhesive force generated by sintering was not enough to cause particle agglomeration. Moreover, the particle agglomeration occurred at temperatures generally below the fusion point of the material [6,14]. Thus, for an actual fluidization system, the mechanism causing sticking may probably vary with experimental conditions. Essentially, the cohesive force causing sticking should be understood as the comprehensive result of all possible interacting forces between particles, which may vary for different particles depending on different situations.

Theoretically, fluidization behavior depends on the balance between the cohesive force (adhering force) between particles and the drag force (separating force) applied to particles by the fluidizing gas. Agglomeration and subsequent defluidization occur when the cohesive force is larger than the drag force. The drag force exerted on particles depends heavily on the gas flow conditions, which could be accurately evaluated [15,16]. While the cohesive force, which is the resistance of particles against the movement, has widely been considered to be determined by interactions between particles including solid/liquid bridging, neck growth, sintering, van der Waals forces, gravity forces, electrostatic forces and so on [17,18]. However, the actual fluidization process is more complicated and varies with experimental conditions, especially when the particles are in a suspended state during the heating process [19,20]. For example, under room temperature, gravity and external frictions tend to be the main resistance, while with raising the temperature to a value under which

†To whom correspondence should be addressed.
E-mail: anzhuoqing@163.com

the properties of particles change considerably, inter-particle cohesive forces caused by surface diffusion, solid/liquid bridging, or sintering become gradually dominant [21-24]. So, it is difficult to determine the magnitude of each force, or that of the entire cohesive force, by measurement or calculation.

Accordingly, a model based on force balance could be proposed to predict the occurrence of defluidization if the inter-particle cohesive force, as well as the total resistance of particles to movement, can be quantitatively characterized. Zhong et al. [7] developed a prediction model based on this principle and predicted the defluidization temperature, where the magnitude of the cohesive force among particles is expressed in terms of solid viscosity. The viscosity of a solid essentially characterizes the degree of surface softening of the solid [25,26]. Generally, the solid surface viscosity decreases with temperature increasing and smaller solid surface viscosity (meaning that the solid surface becomes softer) exhibits a higher adhesion tendency. The decrease of solid viscosity indicates that the increase of cohesive forces caused by particle melting and surface sintering, which may cause particle sticking and agglomeration. The infinite solid viscosity indicates that the solid particles have no tendence to adhere.

The apparent viscosity of particles, proposed by the authors [27], is an alternative way to characterize the magnitude of cohesive forces among particles. Essentially, the concept of apparent viscosity is completely different from that of solid surface viscosity described above. For example, at room temperature, no softening appears on the solid surface means that solid viscosity is infinite. But the interacting forces between particles are not infinite at room temperature. While a particle's apparent viscosity is closer to the viscosity of liquid. As known, the viscosity of a liquid shows the magnitude of the mutual attractive force between liquid molecules, which behave as the resistance of liquids to movement. When an object immersed in the liquid rotates, the rotating object is subjected to the viscous torque of the fluid. By measuring this torque, liquid viscosity can be acquired. Similarly, cohesive forces among solid particles described above are also the main force for particles against movement (causing defluidization in a fluidized bed). When a probe rotates in the solid particles, the torque acting on the probe can reflect the magnitude of cohesive forces. Based on the energy dissipation principle combined with the motion equations of particles, the torque could be acquired; thus, a method for measuring apparent viscosity was developed by the authors [27]. Using this method, the apparent viscosity of iron particles was measured and the results indicated that even the adhesion mechanism of different iron particles is also different; the same apparent viscosity of the particles showed similar resisting ability against movement. Thus, the cohesive force based on the apparent viscosity of solid particles can be reasonably treated as the overall sum of the interacting forces between particles, including gravity, solid/liquid bridging, neck growth, sintering, van der Waals, electrostatic and so on. Using the apparent viscosity of solid particles to characterize the cohesive force between particles is more comprehensive and reasonable. It will provide a new research perspective for the analysis of the interaction force between particles.

In this study, a model based on force balance is put forward to predict the defluidization behavior of particles. In this model, the apparent viscosity of solid particles was used to evaluate the cohesive force. The fluidization behavior of copper particles, including the minimum fluidization velocity and the temperature under which defluidization occurred, was examined in a lab-scale fluidized bed reactor. Further, the comparison between the experimental results and predicted values of this model was discussed.

MODELING

1. Principle

In this model, one particle is considered the study object in a fluidized bed reactor. The forces that act on this particle can be roughly classified into two types: driving force and resistance against movement. The driving force, which promotes the particles to move but against agglomeration, is essentially the same as drag force exerted by flowing gas. The driving force has been evaluated by many studies and through several models [5,7,15,16]. The resistance against movement is characterized using the apparent viscosity of solid particles. Irrespective of the type of force working as resistance, its magnitude can be obtained from the particle apparent viscosity.

Considering the moving, colliding, breaking and coalescing of the particle in a fluidized bed, the following conditions were assumed: (1) The bed material particles are in uniform spherical shape with the same size. (2) The wall effect of fluidized bed is negligible. (3) The cohesive force is used to characterize the resistance of particles against the movement; it can be treated as the overall sum of the interacting forces between particles. (4) The segregation force against agglomeration is the drag force acting on particles owing to bubble motion. (5) Defluidization is a result of a force balance between the total cohesive force between particles and the exertion of drag force applied to particles. (6) If the cohesive force equals or exceeds the drag force, defluidization occurs.

2. Drag Forces on Particles

Generally, it is thought that before fluidization the drag force that the gas exerts on all of the particles obeys Ergun's equation [28]:

$$F_d = 150\frac{(1-\varepsilon)^2}{\varepsilon^3}\times\frac{\mu_g u}{d_p^2} + 1.75\frac{(1-\varepsilon)}{\varepsilon^3}\frac{\rho_g u^2}{d_p} \quad (1)$$

where F_d is the total drag force of a fluidized unit (N/m^3), ε is the voidage of fluidized bed (dimensionless), μ_g is the viscosity of gas (Pa·s), u is the superficial gas velocity (m/s), d_p is the diameter of particle (m), and ρ_g is the density of gas (kg/m^3). Accordingly, for each single particle, the drag force at this stage (F_{d1}) can be described by the following equation [29]:

$$F_{d1} = \frac{\pi F_d d_p^3}{6(1-\varepsilon)} \quad (2)$$

Here, ε, a fluidized bed voidage in Eq. (2), can be obtained by using the following formula:

$$\varepsilon = 1 - \frac{m_0}{\rho_s \pi r_d^2 H} \quad (3)$$

where m_0 is the weight of particles (kg), ρ_s is the particle density (kg/m^3), r_d is the radius of the fluidized bed (m), and H is the height of bed material (m).

When the gas velocity further increases to the minimum fluidization velocity, the fluidized bed begins to gradually expand. And

the pressure drop across the total bed stays at a fixed value. In this case, previous studies [30] have shown that the drag force on each particle no longer obeys Ergun's equation and but rather can be described by Eq. (4), which shows a strong dependence on gas velocity, gas properties and particle size.

$$F_{d2} = \alpha C_d \frac{\pi}{8} d_p^2 \rho_g u^2 \tag{4}$$

where α is a proportionality coefficient that represents the unknown errors in the equation, and C_d is the drag coefficient. C_d has a relationship with the Reynolds number as shown in Eq. (5):

$$C_d = \frac{24}{Re}(1+0.173Re^{0.657}) + \frac{0.413}{1+16300Re^{-1.09}} \tag{5}$$

$$Re = \frac{d_p \rho_g u}{\mu_g} \tag{6}$$

In this study, we assume that the two drag forces (F_{d1}, F_{d2}) are equal at minimum fluidization velocity at room temperature; thus, α can be obtained by the following equation:

$$25\frac{\pi(1-\varepsilon)}{\varepsilon^3}\mu_g u d_p + 0.29\pi\frac{\rho_g u^2 d_p^2}{\varepsilon^3} = \alpha C_d \frac{\pi}{8} d_p^2 \rho_g u^2 \tag{7}$$

Then, placing the value of α in Eq. (4), the drag force under fluidization can be obtained.

3. Cohesive Forces

As described above, the cohesive forces among particles, which behave as the main resistance against movement under high temperature, were characterized by using apparent viscosity. In previous research [27], a measuring method and apparatus were developed to measure the apparent viscosity. In this technique, a blade (shown as Fig. 1(a)) is rotated inside a container of particles. The blade acting as an agitator, and its power number, N_P, is expressed as [31]:

$$N_p = \frac{Q}{\rho_s N_r^3 D^5} = \frac{P \cdot (\pi N_r)}{\rho_s N_r^3 D^5} \tag{8}$$

Here, Q, ρ_s, N_r, D, and P are the specific power consumption (W), the particle density (kg/m^3), the stirring speed of the blade (s^{-1}), the diameter of blade (m), and the torque acting on the blade (Nm), respectively. The flow visualization confirmed that the particles movement was restricted to only the area around the rotating blade and the system can be treated as having laminar flow [31]. The power number is inversely proportional to the Reynolds number [32], Re, shown as the following:

$$N_p \cdot Re = k \tag{9}$$

where k is a constant which represents the characteristics of the shape of the blade. The derivation has also been used for the characterization of fluids such as gas/liquid-solid slurry systems [31,33]. Combining Eq. (8) and (9), the apparent viscosity can be derived from Eq. (10).

$$\eta = A \cdot \frac{P}{\pi N_r D} \tag{10}$$

Here, η is the particle apparent viscosity (Pa·s), and A ($A=\frac{\pi^2}{kD^2}$) is a constant determined by the structure of the blade tip that is independent of other experimental conditions. During experimental measurements with the specified rotating blade, the value of A was obtained by using several reference fluids with known viscosity. Then the particles' apparent viscosity (η) can be obtained using Eq. (10) with fixed P, N_r and D. The details of this process were introduced in a previous publication [27].

Once the apparent viscosity of particles has been obtained, the shear stress acting on the particle lamina can be obtained using Eq. (11). Here, the shear stress on the particle lamina theoretically represents the ability of particles to resist movement. This tends to be treated as the overall results of cohesive forces between particles.

$$Fc = \eta S \dot{\gamma} \tag{11}$$

where Fc is the resistance between particle layers, S represents the contact area between particle layers (m^2), and $\dot{\gamma}$ is the shear rate which the blade applies to the particles (s^{-1}). For the sake of easy determination of $\dot{\gamma}$ and S, the structure of the rotating blade in Fig. 1(a) can be simplified to a structure of double-planes as shown in Fig. 1(b). In this structure, the blade can be treated as one plane and the bottom of the container can be treated as another plane.

Accordingly, the shear rate $\dot{\gamma}$ and contact area S can be obtained through Eq. (12) and (13), respectively.

$$\dot{\gamma} = \frac{r_b}{h}\omega \tag{12}$$

$$S = \pi r_b^2 \tag{13}$$

where r_b is the radius of the blade (m), h is the distance between the blade and the bottom of the container (m), and ω is the angular velocity (rad/s). The number of particles of single particle laminae can be calculated by:

$$n = \frac{\pi (r_b)^2}{d_p^2} \tag{14}$$

Because the blade was rotated inside the container of particles, the shear stress on the blade tip can be considered the comprehensive result of all of the forces interacting between particles in two laminas. Hence the average cohesive force acting on each single particle can be described in the form of:

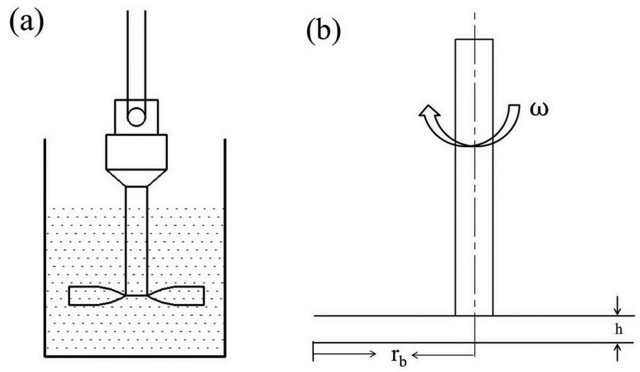

Fig. 1. (a) Schematic diagram of blade rotating in a container of particles; (b) simplified structure of the blade (double-planes).

$$F_p = \frac{\eta \dot{\gamma} d_p^2}{2} \quad (15)$$

EXPERIMENTAL

To examine the feasibility of utilizing the model proposed in this research to predict the defluidization behavior of particles in fluidized beds, two kinds of experiments were carried out in our laboratory. First, the apparent viscosity of solid particles (copper particles were used in this study) was measured using the method described above; then, the fluidization behavior of copper particles in a fluidized bed in our laboratory was investigated. The minimum fluidization velocity and temperature under which defluidization started to occur (referred to as the defluidization temperature in this paper) were obtained.

1. Materials

To simplify the calculations, copper powder (purity >99%, Beijing Xing Rong Yuan Technology Co. Ltd) with a spherical shape was used. The CO_2, Ar, N_2 and H_2 gases used for fluidization were of 99.999% purity and supplied by Beijing Qianxi Gas Chemical Industry Co. Ltd. Before the experiment, the spherical copper powder was sieved. Its pack density was 5,480 kg/m^3 and the mean particle diameter was 61.5 μm. SEM images and particle size distribution of the copper powder are shown in Fig. 2(a) and (b), respectively. As shown in Fig. 2(a), copper particle surface having roughness, the effect of surface roughness on particle cohesion has been widely studied [34,35]. The surface roughness mainly determines the van der Waals forces [36] and capillary force [37]. The apparent viscosity of particles was used to characterize the overall sum of the interacting forces between particles and the van der Waals forces and capillary force has been included. Thus, the influence of surface roughness on the interparticle force has been considered during the measurement process of solid particles' apparent viscosity. And the surface roughness was not discussed separately in this model.

2. Apparatus and Procedures

2-1. Apparent Viscosity Measurement

The apparatus used for measurement of apparent viscosity is shown in Fig. 3(a). A rotating viscometer with a large torque sensor

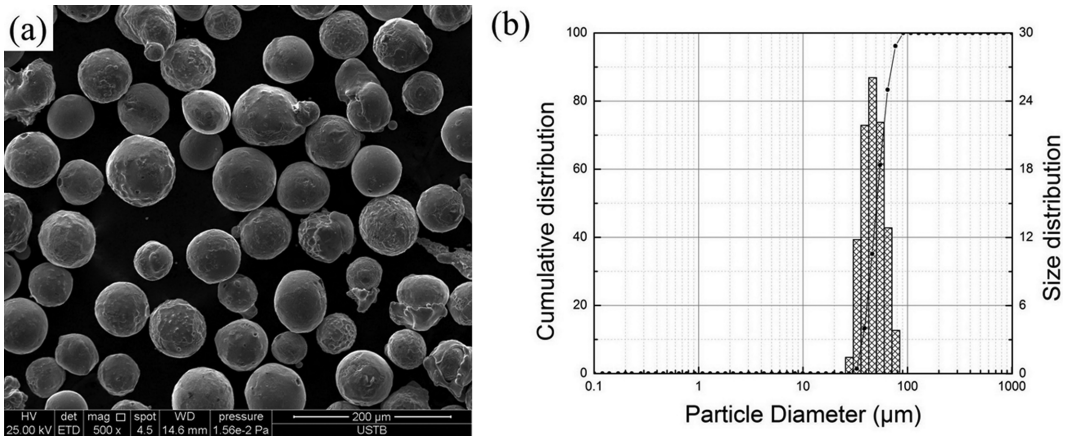

Fig. 2. (a) A SEM microphotograph and (b) particle size distribution of the spherical copper powder.

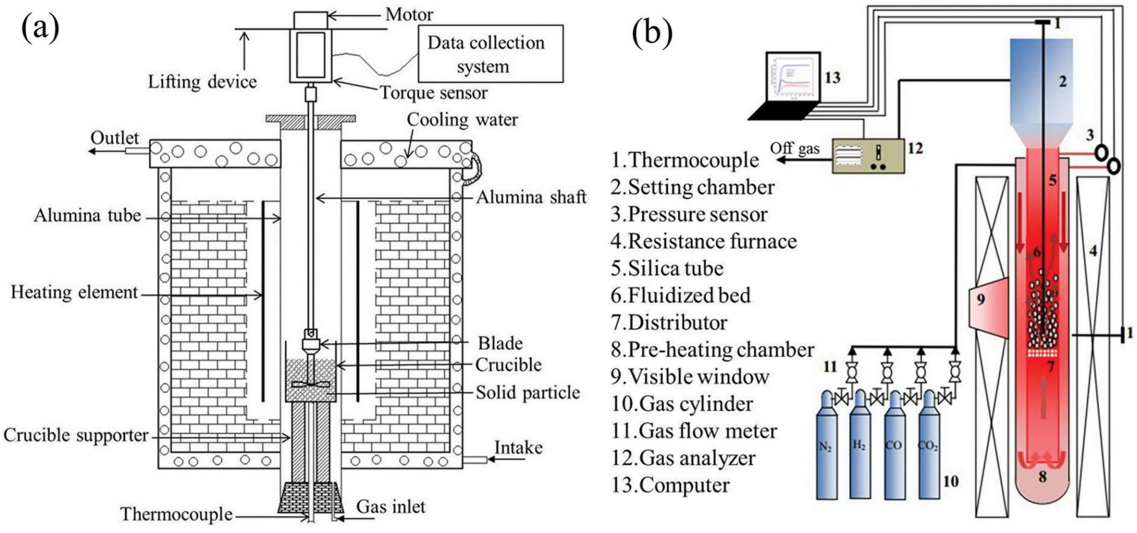

Fig. 3. Schematic diagram of (a) rotational viscometers and (b) visual fluidized bed.

(0-0.5 N·m) was used, and a blade-type probe (Fig. 1(a)) replaced a typical cylinder probe. For each measurement of apparent viscosity, a certain volume of copper particles was added to the alumina crucible (radius: 25 mm and height: 70 mm) after drying. The blade-type probe attached to the alumina shaft was suspended from the torque sensor. When the measurement was carried out at elevated temperature, Ar gas (which had been passed through a column of desiccant to remove H_2O) was inlet into the alumina tube during the measurement to stop the oxidation of copper particles. After an hour, the measurement began at room temperature with a heating rate of 10 °C/min. The blade rotated inside in the crucible filled with solid particles, and the torque measurement was automatically recorded by the data collection system. Then, the particles' apparent viscosity was calculated using Eq. (10).

2-2. Examining Fluidization Behavior

In this research, a visually monitored fluidized bed, whose schematic diagram is shown in Fig. 3(b), was used to characterize the fluidization behavior of copper particles. The reactor is made of two layers of silica tubes placed in a resistively heated tube furnace to preheat the bed. The inner silica tube, with an ID of 30 mm, is the fluidized bed and the outer tube, with an ID of 70 mm, is used to preheat the gas. First, gas flows through the layer between the outer tube and the inner tube for preheating. The gas then flows into a fluidized bed through a silica distributor. The temperature and pressure drop of the fluidized bed were continuously measured using two thermocouples and a pressure sensor. A data acquisition system was used to monitor the temperature and pressure drop of the bed and the air flow rate. The resistance furnace has a window that can be used for visual observation of fluidization.

The minimum fluidization velocities (U_{mf}) of spherical copper particles with different fluidizing gases (CO_2, Ar, N_2 and H_2) were measured at room temperature. First, 50 g of dried spherical copper particles was placed in the visually monitored fluidized bed reactor. Then fluidizing gas (which had been passed through a column of desiccant to remove H_2O) flowed into the fluidized bed through a silica distributor. The gas velocity gradually increased until the bed was completely fluidized and then decreased to zero. At each gas velocity, the pressure drop was recorded when it became stable. Based on the pressure drop measurement, a plot of pressure drop versus gas velocity was acquired. It is generally accepted that the minimum fluidization velocity can be measured regardless of whether velocity is increasing or decreasing [38-40]. Based on previous studies [22], the minimum fluidization velocity is more stable when measured during a decrease in gas velocity. Thus, measurements made during a decrease in gas velocity were employed in this study. The typical plot of pressure drop versus gas velocity for CO_2 in this study is shown in Fig. 4.

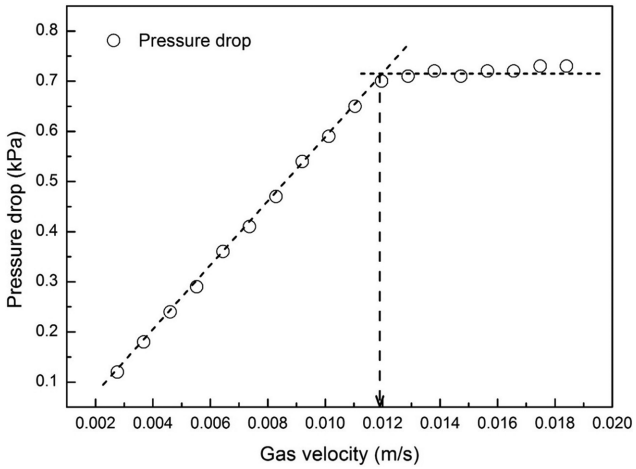

Fig. 4. A diagram of pressure drop versus gas velocity for CO_2.

During defluidization experiments, the same spherical copper particles mentioned above were added to the visually monitored fluidized bed reactor. The bed was fluidized with Ar gas (which had been passed through a column of desiccant to remove H_2O) at a given velocity. The measurement started from room temperature and the temperature was then increased at a rate of 10 °C/min until a sudden drop in bed pressure took place. The sudden drop in bed pressure indicated defluidization. The temperature at which defluidization occurred was recorded as the defluidization temperature. In this study, the defluidization temperatures of spherical copper particles were measured under different Ar gas velocities.

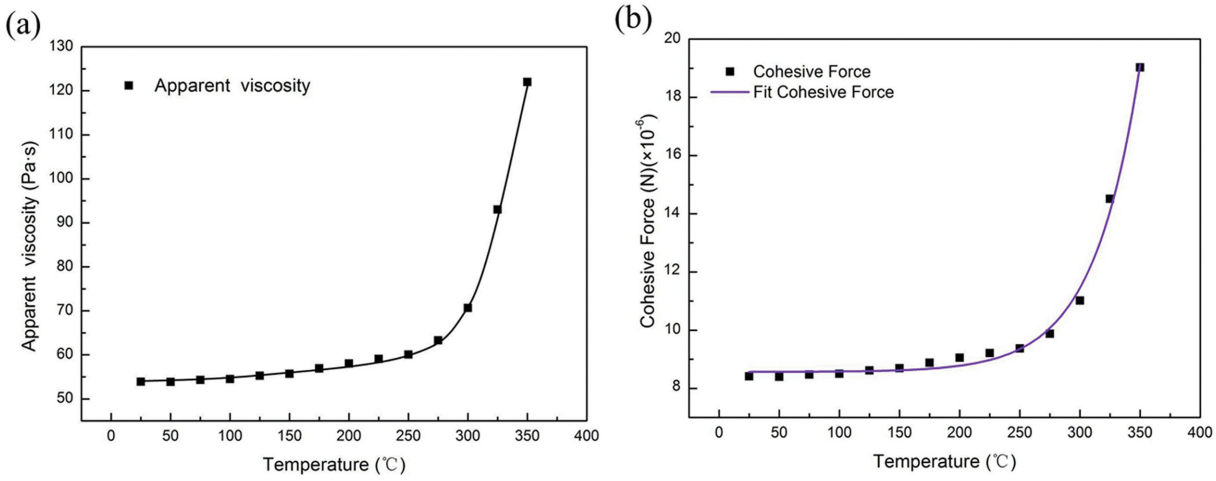

Fig. 5. Effect of temperature on the apparent viscosity (a), and cohesive force of copper powder (b).

RESULTS AND DISCUSSION

1. Apparent Viscosity and Cohesive Force between Copper Particles

The effect of temperature on the apparent viscosity of spherical copper particles is shown in Fig. 5(a). The apparent viscosity of the spherical copper particles gradually increased as the temperature increased. This could be because the cohesive force among the spherical copper particles increased with the increase in temperature. This leads to increased resistance to movement and a trend towards more adhesion. By using the measured apparent viscosity values, the cohesive force between the copper particles can be calculated from Eq. (11). The temperature dependence of cohesive force is shown in Fig. 5(b). The curve shows that the cohesive forces acting on each spherical copper particle are related to temperature. The fit equation is:

$$F_p = 1.2\times10^{-9} e^{\left(\frac{T}{38.6}\right)} + 8.6\times10^{-6} \ (R^2 = 0.99349) \quad (16)$$

Because of limitations in the range of the torque sensor, the cohesive force between copper particles could not be measured at high temperature (>350 °C). In the following section 3, Eq. (16) is used to predict the cohesive force between spherical copper particles at high temperatures (>350 °C).

2. Minimum Fluidization Velocity Prediction

The minimum fluidization velocity is a significant index to characterize the fluidizing properties of particles [39,40]. And a force balance is usually used to predict the minimum fluidization velocity. Zhou et al. [41] proposed a new model to predict the minimum fluidization velocity, in which the drag force would be equal to the sum of the gravity and the effective interparticle forces. Moreover, Anantharaman et al. [42] reported that the lack of understanding of cohesive forces between particles causes the predictions of minimum fluidization velocity to display greater discrepancies. Here, a new model was proposed to predict the minimum fluidization velocity by using the apparent viscosity of particles to characterize the cohesive forces between particles.

In this case, the particles are configured as nearly a fixed bed, and the drag force on those by flowing gas can be expressed as Eq. (2). As shown, the drag force exerted on particles in the fluidized bed increased with the gas velocity increasing. When the cohesive force between particles is less than the drag force, fluidization starts. At the start of fluidization, both of these two forces tend to equal each other. Therefore, we combined Eq. (2) with Eq. (15) to calculate the total drag force (F_d). Then the minimum fluidization velocity was obtained by Eq. (1). The predicted minimum fluidization velocities are listed in Table 1.

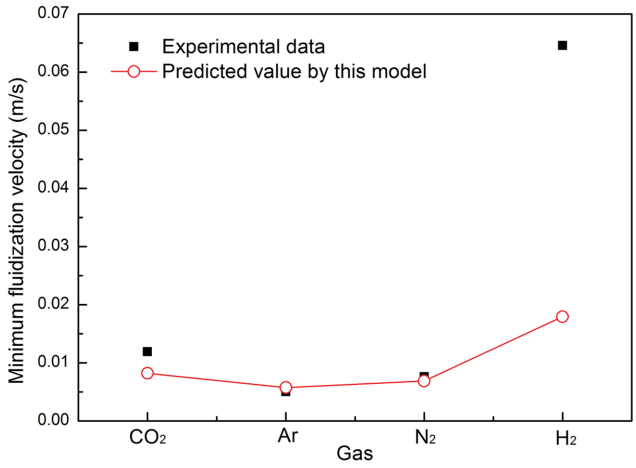

Fig. 6. Comparison of experimental and predicted minimum fluidization velocities.

Fig. 6 shows the comparison of experimental and predicted minimum fluidization velocities under different gas conditions. It indicates that the results predicted by this model agree well with the measured values of the minimum fluidization velocity, of which the relative errors for Ar and N_2 are less than 15% as listed in Table 1. The deviation for CO_2 is around 30%, as the data is accurate to five decimal places, so the deviation is acceptable for this model considering the limitations of the experimental equipment. A larger difference is noted when H_2 is used as fluidizing gas; this could be due to the strong physical or chemical adsorption of H_2 gas onto copper particles. The physical or chemical adsorption of gas would change the surface properties of the particles, thus affecting the force between the particles [43]. The high adsorption activity of H_2 onto metals has been reported by Zhong et al. [14]. It can be inferred that H_2 adsorbed to the copper particles in this study. This suggests that, when the bed is fluidized with H_2, additional H_2 is required to enhance the drag force.

3. Prediction of Defluidization Temperature

The bed pressure drops of spherical copper particles fluidized at different gas velocities (Ar gas) are shown in Fig. 7(a). When a sudden pressure drop occurs, this suggests that defluidization has occurred. As shown in Fig. 7(a), the defluidization temperature increased as the gas velocity increased. The defluidization temperatures corresponding to different gas velocities were 413 °C (0.0236 m/s), 418 °C (0.0354 m/s), 420 °C (0.0389 m/s), 425 °C (0.0486 m/s) and 445 °C (0.0583 m/s). Fig. 7(b) shows the temperature dependencies of the drag forces calculated from Eq. (4) under different gas velocities. It also shows the fitting values of cohesive forces at

Table 1. Experimental and predicted minimum fluidization velocity with different gases

Gas type	Experimental data (m/s)	Predicted data (m/s)	Relative error (%)
CO_2	0.01190	0.00820	31
Ar	0.00503	0.00574	14
N_2	0.00763	0.00686	10
H_2	0.06460	0.01792	72

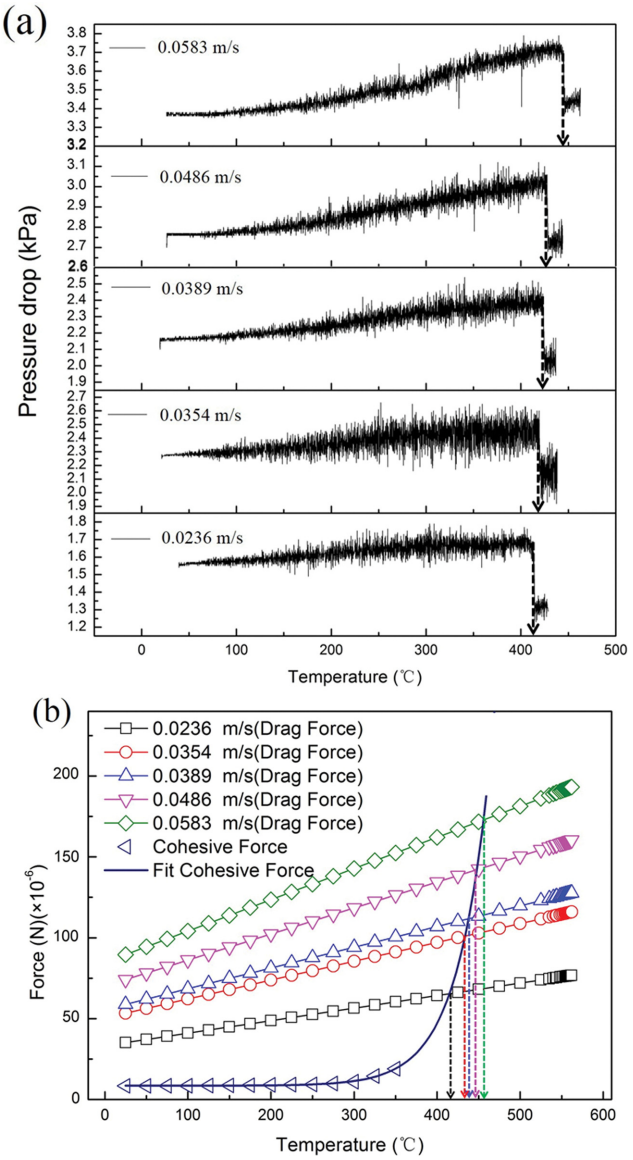

Fig. 7. (a) Dependence of pressure drop of the fluidized bed on temperature and (b) dependence of drag force and cohesive force on temperature.

different temperatures, as calculated using Eq. (16). For each gas velocity, the drag force increases linearly as the temperature increases. The cohesive force increases in slow trend at low temperature (<250 °C). However, the increase in the cohesive force is much more rapid (shown in Fig. 7(b)) than that of drag force at temperatures higher than 250 °C. When the cohesive force is equal to the drag force, defluidization occurs. In this model, the corresponding temperatures are defined as defluidization temperatures. The defluidization temperature predicted by Eq. (4) and Eq. (15) increases with increasing gas velocity. This is because the drag forces exerted on particles increase rapidly (shown in Eq. (4)) with increasing gas velocity, whereas the cohesive force (shown in Eq. (16)) stays the same at a constant temperature. As a result, the cohesive force is smaller than the drag force and the copper particles could not defluidize. Thus, the defluidization temperature increased with gas

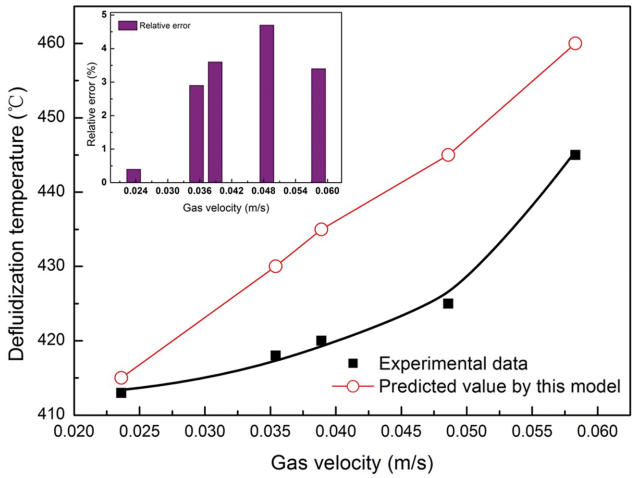

Fig. 8. Comparison of predicted defluidization temperature with experimental data for different gas velocities.

velocity increasing.

The predicted defluidization temperatures by the model against the experimental data obtained from different gas velocities are shown in Fig. 8. It can be seen that the relative error is in the acceptable range of 0 to +5%. The predicted results agree well with the experimental data. Therefore, the model successfully predicted the defluidization temperature as a function of particle apparent viscosity. As a result, it is feasible to use the apparent viscosity of solid particles to characterize the cohesive force between particles for the prediction of defluidization behavior in fluidized beds.

CONCLUSIONS

The apparent viscosity of solid particles was used to characterize the cohesive force between particles. It can be reasonably treated as the overall sum of the interacting forces between particles including gravity forces, solid/liquid bridging, neck growth, sintering, van der Waals forces, electrostatic forces and so on. A model based on a force balance was put forward to predict the minimum fluidization velocity and the defluidization temperature of copper particles in the fluidized bed. The basic principle of this model is that agglomeration and defluidization occur when the cohesive force is larger than the drag force exerted on particles.

The apparent viscosity of spherical copper particles was measured. According to the apparent viscosity, the cohesive force between spherical copper particles was obtained. The cohesive force increases with increasing temperature, and its relationship with temperature is as follows:

$$F_p = 1.2\times10^{-9} e^{\left(\frac{T}{38.6}\right)} + 8.6\times10^{-6}$$

The minimum fluidization velocity and defluidization temperature of spherical copper particles in the fluidized bed were measured in the laboratory. Both the results predicted by this model agree well with the experimental data, confirming the reliability of using the apparent viscosity of solid particles to predict the fluidization behavior of fluidized beds.

ACKNOWLEDGEMENTS

The authors would like to acknowledge the financial support from National Natural Science Foundation of China (No. 51234001), Natural Science Foundation of Inner Mongolia Autonomous Region (No. 2019BS05018), Research Program of Science and Technology at Universities of Inner Mongolia Autonomous Region (No. NJZY19128), and Inner Mongolia University of Science and Technology Innovation Fund (No. 2019QDL-B17).

DECLARATION OF COMPETING INTEREST

The authors declare that they have no conflict of interest.

REFERENCES

1. F. Karimi, M. Haghshenasfard, R. Sotudeh-Gharebagh, R. Zarghami and N. Mostoufi, Adv. *Powder Technol*., **29**, 3145 (2018).
2. J. R. Lee, Y. H. Kim and Y. S. Won, *Korean J. Chem. Eng*., **38**, 1791 (2021).
3. I. Mishra, P. Liu, A. Shetty and M. Hrenya, *Chem. Eng. Sci*., **214**, 115422 (2020).
4. Y. Zhou, Q. Shi, Z. Huang, J. Wang and Y. Yang, *Chem. Eng. J*., **330**, 840 (2017).
5. J. Li, J. Kong, S. He, Q. Zhu and H. Li, *Chem. Eng. Sci*., **177**, 455 (2018).
6. M. Komatina and H. W. Gudenau, *J. Metall*., **10**, 309 (2004).
7. Y. Zhong, Z. Wang, Z. Guo and Q. Tang, *Powder Technol*., **249**, 175 (2013).
8. H. Lu, J. Cao, D. Macri, X. Guo, H. Liu and X. Gong, *Powder Technol*., **380**, 106 (2021).
9. B. J. Skrifvars, M. Hupa, R. Backman and M. Hiltunen, *Fuel*, **73**, 171 (1994).
10. C. L. Lin, M. Y. Wey and C. Y. Lu, *Powder Technol*., **161**, 150 (2006).
11. J. M. Valverde and A. Castellanos, *Chem. Eng. J*., **140**, 296 (2008).
12. J. P. K. Seville, H. Silomon-Pflug and P. C. Knight, *Powder Technol*., **97**, 160 (1998).
13. P. C. Knight, J. P. K. Seville, H. Kamiya and M. Horio, *Chem. Eng. Sci*., **55**, 4783 (2000).
14. Y. Zhong, Z. Wang, Z. Guo and Q. Tang, *Powder Technol*., **230**, 225 (2012).
15. X. Gong, B. Zhang, Z. Wang and Z. Guo, *Metall. Trans. B*., **45**, 2050 (2014).
16. J. He, Y. Zhao, Y. He, P. Walzel, G. Schaldach and C. Duan, *Powder Technol*., **241**, 204 (2013).
17. T. Mikami, H. Kamiya and M. Horio, *Powder Technol*., **89**, 231 (1996).
18. J. P. K. Seville, C. D. Willett and P. C. Knight, *Powder Technol*., **113**, 261 (2000).
19. E. J. Hinch, *J. Fluid Mech*., **686**, 1 (2011).
20. L. G. Gibilaro, K. Gallucci, R. Di Felice and P. Pagliai, *Chem. Eng. Sci*., **62**, 294 (2007).
21. C. Lei, Q. Zhu and H. Li, *Chem. Eng. Sci*., **118**, 50 (2014).
22. C. L. Lin, M. Y. Wey and S. D. You, *Powder Technol*., **126**, 297 (2002).
23. X. S. Wang and M. J. Rhodes, *Chem. Eng. Sci*., **59**, 215 (2004).
24. R. Yamazaki, N. S. Han, Z. F. Sun and G. Jimbo, *Powder Technol*., **84**, 15 (1995).
25. M. F. M. Osborne, *Kolloid-Zeitschrift und Zeitschrift für Polymere*, **224**, 150 (1968).
26. G. Tardos, D. Mazzone and R. Pfeffer, *Can. J. Chem. Eng*., **62**, 884 (1984).
27. Y. Zhang, Z. An, H. Bai, Q. Li and Z. Guo, *Powder Technol*., **284**, 279 (2015).
28. S. Ergun, *Chem. Eng. Prog*., **48**, 89 (1952).
29. J. H. Kuo, K. Shih, C. L. Lin and M. Y. Wey, *Powder Technol*., **224**, 395 (2012).
30. R. Turton and O. Levenspiel, *Powder Technol*., **47**, 83 (1986).
31. Y. Komoda, K. Nakashima, H. Suzuki and H. Usui, *Adv. Powder Technol*., **17**, 333 (2006).
32. C. Torrez and C. André, *Chem. Eng. Technol*., **21**, 599 (1998).
33. P. K. Biswas, K. M. Godiwalla, D. Sanyal and S. C. Dev, *Mate. Des.*, **23**, 511 (2002).
34. H. R. Moutinho, C. S. Jiang, B. To, C. Perkins, M. Muller, M. M. Al-Jassim and L. Simpson, *Energ. Mat. Sol. C*., **172**, 145 (2017).
35. C. S. Sandeep and K. Senetakis, *Materials*, **11**, 217 (2018).
36. J. Katainen, M. Paajanen, E. Ahtola, V. Pore and J. Lahtinen, *J. Colloid Interface Sci*., **304**, 524 (2006).
37. A. Ata, Y. I. Rabinovich and R. K. Singh, *J. Adhes. Sci. Technol*., **16**, 337 (2002).
38. K. Noda, S. Uchida, T. Makino and H. Kamo, *Powder Technol*., **46**, 149 (1986).
39. D. Gidaspow, *Multiphase flow and fluidization: continuum and kinetic theory descriptions*, Academic Press (1994).
40. C. Y. Wen and Y. H. Yu, *AIChE J*., **12**, 610 (1966).
41. Y. Zhou and J. Zhu, *Chem. Eng. J*., **1**, 402 (2020).
42. A. Anantharaman, R. A. Cocco and J. W. Chew, *Powder Technol*., **454**, 323 (2018).
43. T. Kai, T. Kamei and T. Takahashi, *AIChE J*., **44**, 491 (1998).